Forschungszentrum Karlsruhe
in der Helmholtz-Gemeinschaftt

Wissenschaftliche Berichte
FZKA 7252

Fracture Mechanical Experiments on EUROFER 97 and MANET II Mini-bar Specimens

Final Report for Task TW5-TTMS 005-D04

E. Gaganidze, B. Dafferner, J. Aktaa

Institut für Materialforschung
Programm Kernfusion
Association Forschungszentrum Karlsruhe / EURATOM

August 2006

Forschungszentrum Karlsruhe

in der Helmholtz-Gemeinschaft

Wissenschaftliche Berichte

FZKA 7252

Fracture Mechanical Experiments on EUROFER 97 and MANET II Mini-bar Specimens

Final Report for Task TW5-TTMS 005-D04

E. Gaganidze, B. Dafferner and J. Aktaa

Institut für Materialforschung

Programm Kernfusion

Association Forschungszentrum Karlsruhe / EURATOM

Forschungszentrum Karlsruhe GmbH, Karlsruhe

2006

This work, supported by the European Communities under the contract of Association between EURATOM and Forschungszentrum Karlsruhe, was carried out within the framework of the European Fusion Development Agreement. The views and opinions expressed herein do not necessarily reflect those of the European Commission.

Forschungszentrum Karlsruhe GmbH
Postfach 3640, 76021 Karlsruhe

Mitglied der Hermann von Helmholtz-Gemeinschaft
Deutscher Forschungszentren (HGF)

ISSN 0947-8620

urn:nbn:de:0005-072521

Abstract

This report summarizes Fracture Mechanical (FM) experiments carried out under the contract of the European Fusion Development Agreement (EFDA), subtask TW5-TTMS-005-D04 for supporting the modeling work on size effects in ductile and ductile to brittle transition region performed within a task TW5-TTMS-005-D3. Quasi-static *three-point-bend* (3PB) experiments have been performed on the European reference RAFM steel EUROFER 97 and on a martensitic steel MANET II.

The crack resistance curves have been constructed from the original fracture mechanical data in the ductile and ductile to brittle transition regions. Additionally, in the ductile region, where complexity of the three dimensional fracture surfaces prevented an explicit quantitative assessment of the crack extension, the validity of the failure assessment diagram (R6) has been verified for RAFM steel EUROFER 97.

Bruchmechanische Untersuchungen an EUROFER 97 und MANET II miniaturisierten Proben

Zusammenfassung

In diesem Bericht werden die bruchmechanischen Untersuchungen zusammengefasst, welche zur Unterstützung von Modellierungsarbeiten von Größeneffekten in duktilen und spröd-duktilen Übergangsbereichen (Subtask TW5-TTMS-005-D03) im Rahmen des Europäischen Abkommens zur Entwicklung der Fusionsforschung (EFDA), Subtask TW5-TTMS-005-D04 durchgeführt wurden. Es wurden quasi-statische Drei-Punkt-Biegeversuche (3PB) an dem Europäischen RAFM Referenzstahl EUROFER 97 und an dem martensitischen Stahl MANET II durchgeführt.

Die Risswiderstandskurven wurden durch die Auswertung von bruchmechanischen Versuchen in duktilen und spröd-duktilen Übergangsbereichen erstellt. Im duktilen Bereich, wo die Komplexität der drei dimensionalen Bruchflächen eine explizite quantitative Auswertung des Risswachstums verhinderte, wurde zusätzlich die Gültigkeit der Auslegungskurve (R6) an dem RAFM Stahl EUROFER 97 überprüft.

CONTENTS

TABLES

Figures

1 Objective

The development of a convenient model for fracture mechanics (FM) experiments is a huge challenge. Finding of scaling factors, which would allow prediction of a crack resistance curve of a standard specimen on the basis of the results obtained on miniaturized specimens, is of vital importance for qualification of structure materials of future fusion reactors. To support modelling work on size effects in the ductile and ductile-to-brittle transition region of structure materials carried out in task TW5-TTMS-005-D3 several fracture mechanics experiments are needed.

Various types of FM specimens, e.g. standard, sub-sized and miniaturized pre-cracked Charpy-V specimens [1],[2], standard and miniaturised compact tension specimens [3], the cylindrical bar specimens pre-cracked by rotary fatigue [1], etc. are intensively used for FM examination. The present work generates experimental data for TW5-TTMS-005-D3 verifying miniaturized *three-point-bend* specimens developed in [2] for determination of quasi-static fracture toughness in the ductile and ductile-to-brittle transition regions.

2 Experimental

An industrial batch of the European reduced activation ferritic martensitic (RAFM) steel EUROFER 97 was produced by Böhler Austria GmbH. The chemical composition of the steels along with the heat numbers are indicated in Table 6-1. A 25 mm thick plate in the as-delivered state has been chosen for specimen preparation. The steel shows ductile failure at room temperature as already shown in [2].

Another steel examined in this work is a martensitic steel MANET II. After a proper heat treatment, see Table 6-2, MANET II shows failure in the ductile-to-brittle transition region at room temperature.

Mini-bar specimens of KLST type (3x4x27 mm^3) have been produced parallel to the rolling direction of the material plates (L-T orientation). Two types of starter notches, i.e. U- and V-notches have been examined in the current experiments see Fig. 6-1 and Fig. 6-2.

The specimens have been fatigue pre-cracked by combined dynamic and static bending by means of a resonant testing machine. The applied bending moments were kept well below the maximum bending moment of

$$M_{\max} = \sigma_y \frac{B(W - a_0)^2}{6} \qquad (1)$$

with σ_y being the yield stress, B the specimen thickness, W the specimen width and a_0 the crack length. The most specimens have been pre-cracked to nominal relative crack lengths of $a_0/W \sim 0.25$. In order to study the influence of the initial crack length, however, some of the specimens have been pre-cracked up to $a_0/W \sim 0.36$. Furthermore, to improve the constraint state near the crack tip, part of the specimens has been side grooved after fatigue pre-cracking.

Room temperature quasi-static *three-point-bend* (3PB) testing has been performed with a servo-hydraulic testing machine Hydropuls®-VHS®-50 (Schenk/Instron). Displacement controlled bending of the specimens have been performed with typical displacement rates between 2-5 mm/min.

A multi-specimen method has been applied for determination of the critical J-integral [4]. For this purpose the specimens have been loaded to different deformation levels to obtain different crack-growth. The deformation energy (U) was determined by integration of the load vs. deflection curve. J-integral has been calculated according to relation

$$J = \frac{2U}{B(W - a_0)} \quad (2).$$

For assessment of the crack extension, the specimens have been heat tinted after each experiment (310 °C/20 min) and broken at low temperatures. Original crack length, crack-tip blunting (δ_{tx}) and stable crack extension was measured at nine equally spaced points centered about the specimen centerline in order to determine an average initial crack length a_0 and an average stable crack extension Δa. Alternatively, when necking of fracture surface prevented an assessment of crack extensions near the root of side grooves (or surfaces of plane-sided specimens), the two outermost measurements of crack extensions have been performed at deeper positions, whereas the remaining seven of nine measurements were carried out at seven equally spaced points, see Fig. 6-7 for crack extension measurement points. J-integral vs. Δa curves have been constructed and fitted with a power law function

$$J = C(\Delta a)^p \quad (3)$$

with C and p as fitting parameters. Critical $J_{0.2}$ value (i.e. J integral at 0.2 mm crack extension) has been determined by analyzing the fitting curve (Eq. (3)). Additionally, linear fitting of J-integral vs. Δa curve has been applied in order to estimate J_{IC} – critical J integral at the onset of stable crack growth. Only experimental points obeying $0.15 \leq \Delta a \leq 1.5$ mm validity criteria for a crack extension have been involved in the both fitting procedures.

Fracture toughness K_{IC} has been calculated from the determined J_{IC} according to the relationship

$$K_{IC} = \sqrt{\frac{J_{IC} E}{1 - \nu^2}} \quad (4).$$

Here E is the Young's modulus for plane stress and ν (≈0.3) is the Poisson's ratio.

Originally developed for high strength ferritic steels, the defect assessment procedure R6 was proved to be also applicable for austenitic steels [5]. Particularly, it was demonstrated that the approximate material-specific curve, termed option 2 which is derived from uniaxial stress/strain data describes well the fracture behaviour of parent austenitic steels and their welds in a wide temperature range [5].

To apply the R6 procedures, calculation of two parameters K_r and L_r is necessary for a particular load P

$$K_r = \frac{K_I(P, a_0)}{K_{IC}} \tag{5}$$

$$L_r = \frac{P}{P_L(a_0, \sigma_y)} \tag{6}$$

where K_I is the elastic stress intensity factor

$$K_I = \frac{PS}{B\sqrt{W^3}} f\left(\frac{a_0}{W}\right) \tag{7}$$

with S being the span of bend fixtures (distance between supports) and $f(a_0/W)$ being the geometry function for bending [6]. $P_L(a_0,\sigma_y)$ is the *plastic collapse* load assuming an elastic-ideal plastic behaviour with a flow stress equal to material yield stress (σ_y). Component failure is avoided if (i) there is avoidance of fracture under linear elastic condition ($K_r \leq 1$) and (ii) avoidance of failure by *plastic collapse* ($P \leq P_L(a_0,\sigma_F)$ or equivalently $L_r \leq L_r^{max}$). $P_L(a_0,\sigma_F)$ is the *plastic collapse* load assuming an elastic-ideal plastic behaviour with a flow stress (σ_F) which is often determined taking into account the material hardening as the average of the ultimate tensile strength (σ_u) and the yield stress (σ_y), i.e. $\sigma_F=(\sigma_u+\sigma_y)/2$. Consequently, L_r^{max} equals σ_F/σ_y. For side grooved specimens the thickness B in Eq. (7) is replaced by $(BB_N)^{1/2}$ [7], where B_N is a net thickness of a specimen (i.e. distance between the roots of side grooves).

It has been shown that the option 1 curve of R6 that is an empirical fit to option 2 curve gives a reliable failure assessment for a variety of materials [5]. The option 1 curve is given by

$$f_1(L_r) = K_r = \left[1 - 0.14L_r^2\right]\left[0.3 + 0.7\exp\left(-0.65L_r^6\right)\right] \tag{8}.$$

For a *three-point-bend* specimen with an original crack length of a_0 the *plastic collapse* load can be calculated by

$$P_L(a_0, \sigma_y) = \frac{4}{3}\frac{BW^2}{S}\sigma_y\left(1 - \frac{a_0}{W}\right)^2 \tag{9}.$$

For side grooved specimens the thickness B in Eq. (9) is replaced by $(BB_N)^{1/2}$.

3 Results and Discussion

3.1 EUROFER 97

All EUROFER 97 specimens exhibited ductile failure at RT. Fig. 6-3 shows optical images of the fracture surfaces of one tested specimen (EF37). A complex three dimensional fracture surfaces with significant inhomogeneous plastic deformation is observed for EUROFER 97 specimen. Scanning electron microscopy (SEM) image of a fracture surface is shown in Fig.

6-4 (top). Fig. 6-4 (bottom) shows a fracture surface profile extracted along a straight line along expected crack propagation. The examination of the surface profile reveals a complex zig-zag crack-propagation preventing a quantitative assessment of the stable-crack extension. Such behaviour was representative for all tested EUROFER 97 specimens without side grooves and prevented construction of crack resistance curves.

In order to improve the constraint state near the crack tip part of the EUROFER 97 specimens were side grooved after fatigue pre-cracking ($a_0/W \approx 0.2$). Fig. 6-5 shows optical images of one tested side grooved specimen (EF56). A complex ductile crack growth is seen similar to the results obtained on the specimens without side grooves (e.g. Fig. 6-3).

Selected EUROFER 97 specimens have been fatigue pre-cracked up to initial lengths of $a_0/W \approx 0.34$-0.36 and side grooved afterwards. Fig. 6-6 shows one representative specimen after *three-point-bend* testing together with a corresponding fracture surface. Though not a plain fracture surface is obtained, a somewhat better crack growth picture is seen compared to specimens with shorter fatigue pre-cracks (i.e. Fig. 6-3, Fig. 6-5).

For construction of the crack resistance curves for the specimens with $a_0/W \approx 0.34$-0.36, the fracture surfaces have been analysed with respect to in-plane Δa^* components of the stable crack extensions Δa, see for example Fig. 6-7. Assessed initial crack lengths, in-plane stable crack-extensions (Δa^*) together with specimen deformation energies and J-integral values are summarized in Table 6-3. Five out of seven specimens obeyed $0.15 \leq \Delta a \leq 1.5$ mm criteria for the crack extension. Fig. 6-8 shows the crack resistance curve along with a least square fit with Eq. (3). The best fit was obtained with parameters C=726 and p=0.53. Critical value of J integral at 0.2 mm stable crack extension was determined as $J_{0.2}$ = 310 N/mm. The determination of a critical value of J integral at the onset of stable crack growth yielded J_{IC}=249 N/mm (or equivalently K_{IC}=240 MPa·m$^{0.5}$). The ASTM validity criteria on specimen thickness $B \geq B_{min}$= 25 (J_{IC} /σ_y) for J_{IC} determination is not fulfilled with B_{min}=11.56 mm. The obtained fracture toughness (240 MPa·m$^{0.5}$) is slightly lower than fracture toughness obtained on larger specimens through analysis of the crack resistance (J-Δa) curves [2]. Indeed, K_{IC} of 258 and 256 MPa·m$^{0.5}$ have been obtained in [2] on 9x18x92 mm^3 bend bar specimens without and with side grooves, respectively.

The validity of the failure assessment diagram, the so called option 1 curve (Eq. (7)) has been verified for EUROFER 97. For this purpose selected pre-cracked EUROFER 97 specimens with and without side groves have been deformed to load levels (P_c) leading to a macroscopic appearance of crack initiation (i.e. crack extension less than 70 µm). Fig. 6-9 shows exemplarily a load vs. displacement curve for EF55 together with optical images revealing a macroscopic appearance of crack initiation.

Stress intensity factor for a load level leading to a macroscopic crack initiation, i.e. $K_I(P_c)$ was calculated with Eq. (7). Assuming the validity of the option 1 curve shown in Fig. 6-10, fracture toughness (K_{IC}) was obtained from Eq. (5). The results for selected EUROFER 97 specimens are summarized in Table 6-4. Fracture toughness values obtained on the basis of option 1 curve show relatively narrow scattering band (within 8.4% of the mean value of 250 MPa·m$^{0.5}$) and are in line with fracture toughness data obtained on larger EUROFER 97

bend bar specimens [2]. This observation proves the assumption of validity of option 1 curve for ferritic martensitic steel EUROFER 97.

3.2 MANET II

All MANET II specimens exhibited failure in the ductile-to-brittle transition region. Fig. 6-11 shows optical image of the fracture surface of one MANET II specimen (H709). Characteristic areas, such as, starting notch, fatigue pre-crack, blunting zone and stable crack extension can be identified. Estimated stable crack-extensions together with specimen deformation energies and J-integral values are summarized in Table 6-5. Five out of nine specimens obeyed $0.15 \leq \Delta a \leq 1.5$ mm criteria for the crack extension. Fig. 6-12 shows the crack resistance curve along with a least square fit with Eq. (3). The best fit was obtained with parameters C=678 and p=0.43. Critical value of J integral at 0.2 mm stable crack extension was determined as $J_{0.2}$ = 339 N/mm. The determination of a critical value of J integral at the onset of stable crack growth yielded J_{IC}=250 N/mm. The ASTM validity criteria on specimen thickness $B \geq B_{min}$= 25 (J_{IC} /σ_y) for J_{IC} determination is not fulfilled with B_{min}=8.19 mm. Remarkably, determined $J_{0.2}$ and J_{IC} values agree well with the results obtained in [2] on 3x6x30 mm^3 *three-point-bend* specimens (327 and 249 N/mm, respectively). Comparatively, J_{IC} value of 150 N/mm was obtained on larger 3PB specimens (9x18x92 mm^3) in [2].

4 Summary

Quasi-static *three-point-bend* (3PB) experiments have been performed on the European reference RAFM steel EUROFER97 and on a martensitic steel MANET II.

All EUROFER 97 specimens exhibited ductile failure at room temperature. The complexity of the three dimensional fracture surfaces did not allow an explicit quantitative assessment of the crack extension. In-plane components of the crack extension have been assessed for construction of a crack resistance (J-Δa) curve. K_{IC}=240 MPa·m$^{0.5}$ determined this way agree well with the literature data on larger specimens. The validity of the failure assessment procedure R6 has been verified for a number of EUROFER 97 specimens. K_{IC} values calculated under assumption of option 1 curve of R6 procedure are sensibly independent of specimen geometry (i.e. “U” and “V” starter notches), constraint state (with and without side grooves) and initial crack length ($0.20 \leq a_0/W \leq 0.36$) and agree well with fracture toughness results obtained on larger EUROFER 97 bend bar specimens.

All MANET II specimens exhibited failure in the ductile-to-brittle transition region. The analysis of the crack resistance curve (J-Δa), constructed from the original fracture mechanical data, resulted $J_{0.2}$ = 339 N/mm and J_{IC}=250 N/mm in a good agreement with literature results on 3x6x30mm^3 specimens.

Acknowledgement

The authors would like to express their thanks to Ms. Dr. E. Materna-Morris for TEM analysis of a fracture surface.

5 References

[1] E. Lucon, Material damage evaluation and residual life assessment of primary power plant components for long-term operation using specimens of non-standard dimensions, La Revue de Métallurgie-CIT/Science at Génie des Matériaux, Décembre 2001, 1079-1091.

[2] H.-C. Schneider, Entwicklung einer miniaturisierten bruchmechanischen Probe für Nachbestrahlungsuntersuchungen, Doktorarbeit Uni-Karlsruhe 2005, FZKA 7066.

[3] J. Rensman, NRG Irradiation Testing: Report on 300°C and 60°C Irradiated RAFM Steels, Petten 2005, 20023/05.68497/P.

[4] ASTM E813-89, Standard Test Method for J_{IC}, A Measure of Fracture Toughness, Annual Book of ASTM Standards, Section 3, pp 633-647, ASTM West Conshohocken, USA, 1996.

[5] R.A. Ainsworth, Failure assessment Diagrams for use in R6 assessments for austenitic components, Int. J. Pres. Ves. & Piping 65 (1996) 303-309.

[6] T. Fett, D. Munz, Stress Intensity Factors and Weight Functions, *Computational Mechanics Publications*, *Advances in Fracture Series*, Southampton UK and Boston, 1997.

[7] ASTM Designation: E1921-97, Standard Test Method for Determination of Reference Temperature, T_0, for Ferritic Steels in the Transition Range, ASTM, 100 Barr Harbor Drive, West Conshohocken, PA 19428-2959, USA, 1998.

6 Appendix

6.1 Material chemical composition

MATERIAL	EUROFER97	MANET II
Heat	83697	50805
Cr	8.91	9.94
W	1.08	n.s.
Mn	0.48	0.79
V	0.2	0.22
Ta	0.14	n.s.
C	0.12	0.1
Si	0.04	0.14
P	0.005	<0.006
S	0.004	<0.007
Ni	0.02	0.66
Mo	<0.001	0.59
Nb	0.0017	0.14
Al	0.009	<0.02
B	0.001	0.007
N	0.02	0.023
O	0.0008	n.s.
Co	0.006	<0.02
Cu	0.0015	<0.01
Zr	<0.005	0.034
Ti	0.006	n.s.
As	<0.005	n.s.
Sb	<0.005	n.s.
Sn	<0.005	n.s.
Fe	balance	Balance

Table 6-1 Material chemical composition in wt% (n.s. not specified).

6.2 Heat-treatment conditions

Material	**Heat treatment**
EUROFER97	980°C/0.5h + 760°C/1.5h
MANET II	965°C/2.0h + 1075°C/0.5h + 700°C/2.0h

Table 6-2 Material heat treatment conditions.

6.3 Specimen geometry

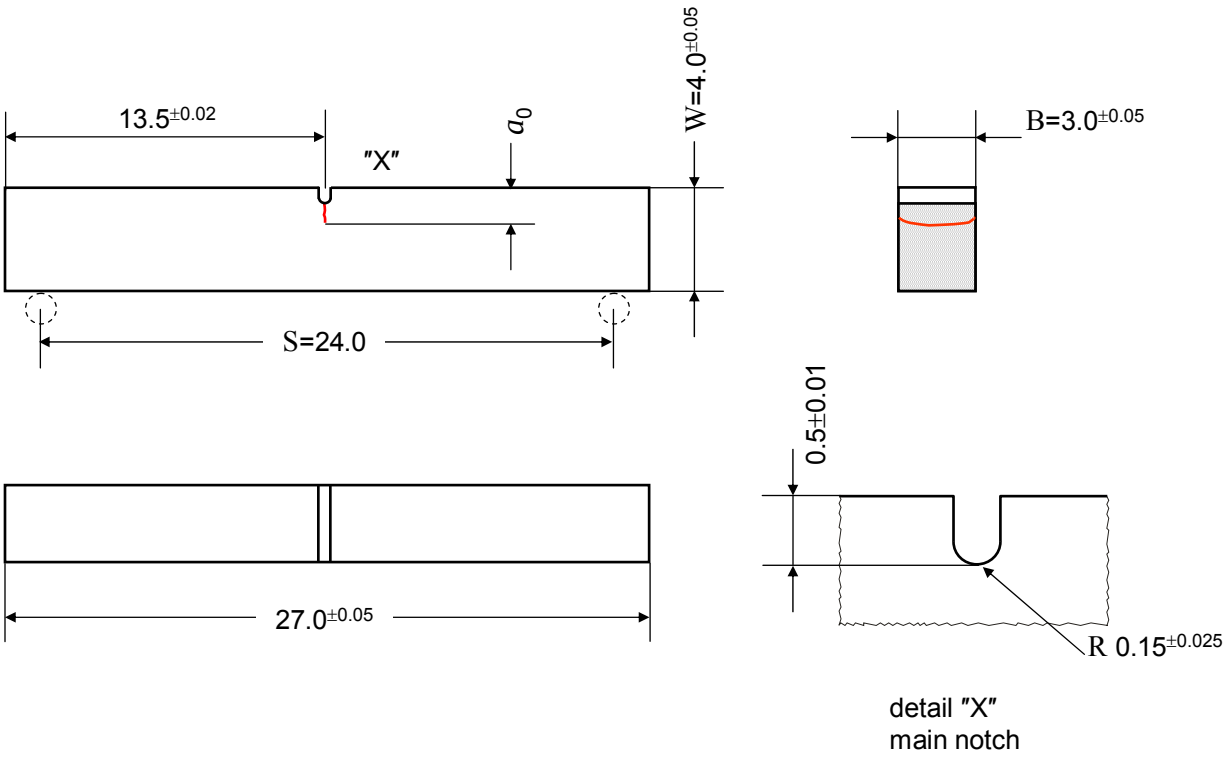

Fig. 6-1 Mini-bar KLST specimen with “U” type starter notch. All dimensions in mm.

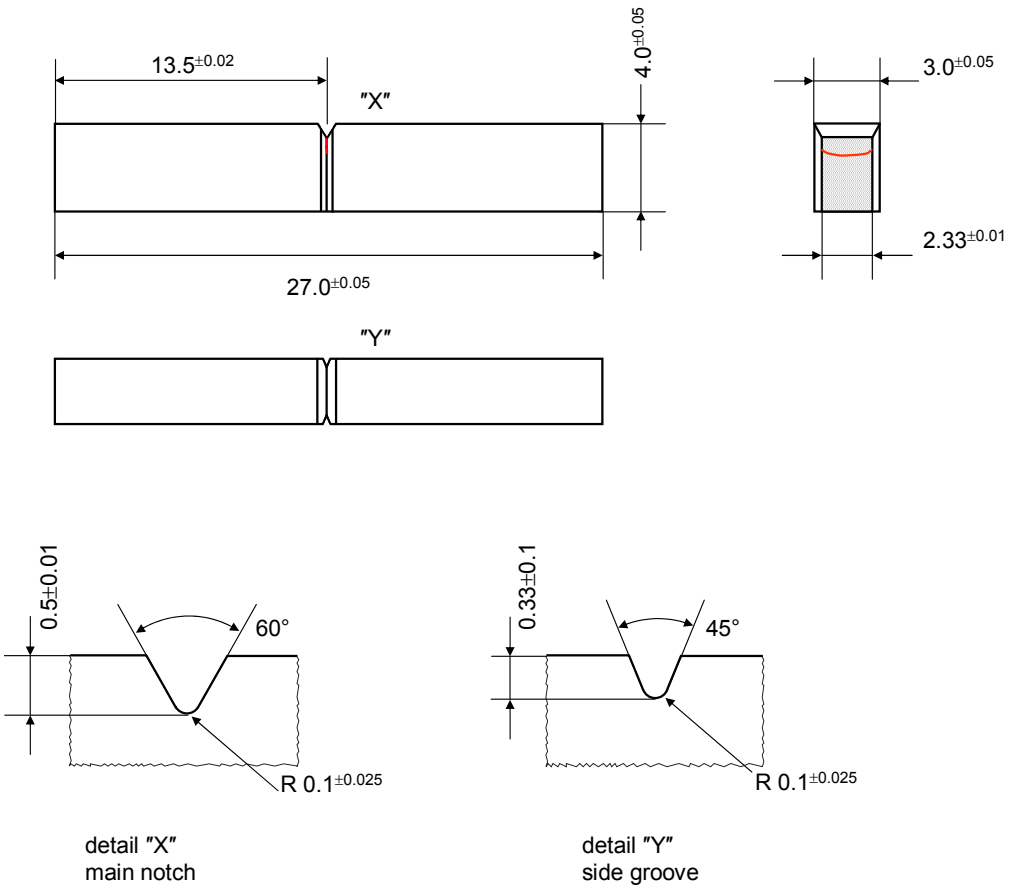

Fig. 6-2 Mini-bar KLST specimen with “V” type starter notch and side grooves. Side grooves are machined after fatigue pre-cracking of the specimen. All dimensions in mm.

6.4 Experimental Results – EUROFER 97

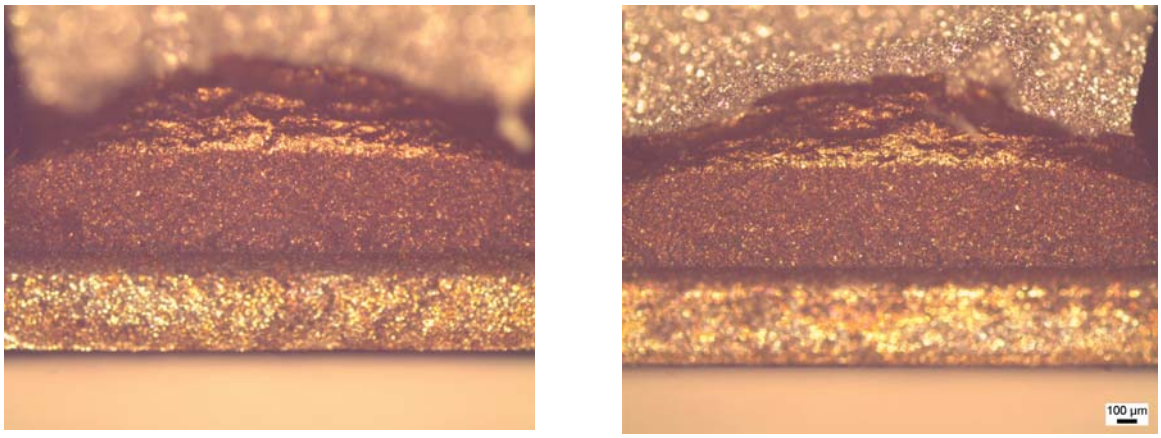

Fig. 6-3 Fracture surfaces of mini-bar EUROFER 97 specimen (EF37); Starter notch type “U”; $a_0/W \approx 0.24$.

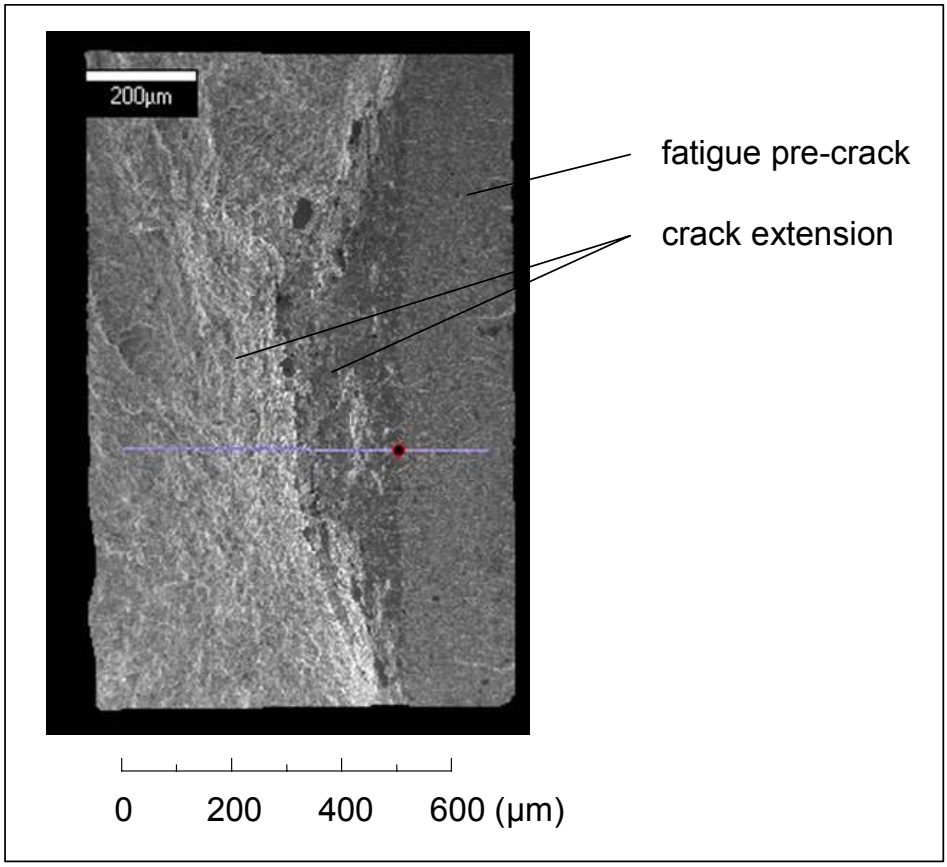

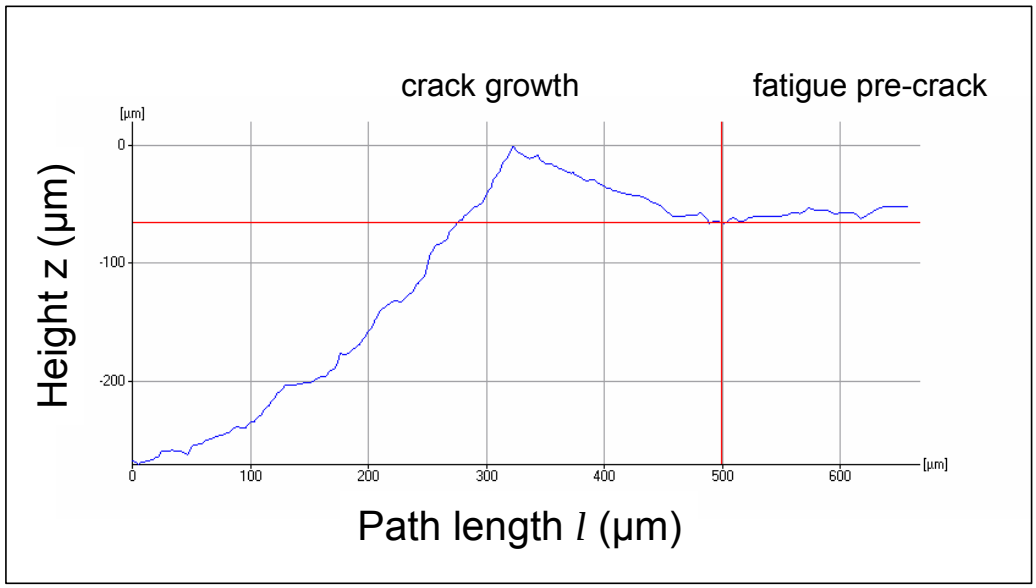

Fig. 6-4 (top) SEM image of a fracture surface of mini-bar EUROFER 97 specimen (EF37), see also Fig. 6-3; The abscissa scale for the profile graph (bottom) is also indicated; (bottom) Fracture surface profile extracted along the path indicated in the top image by a straight line.

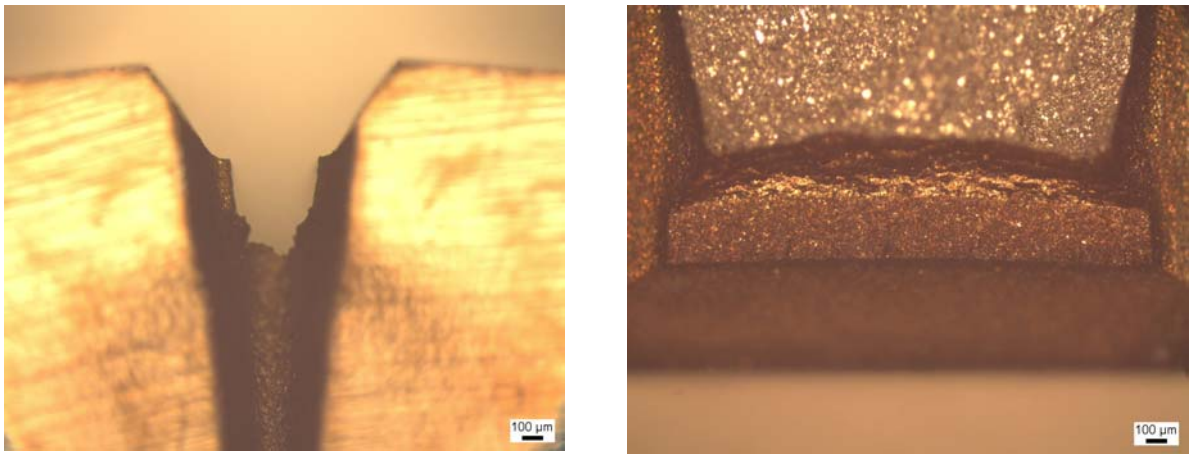

Fig. 6-5 (left) Side view of side grooved mini-bar EUROFER 97 specimen (EF56); Starter notch type ″V″; $a_0/W \approx 0.2$; (right) Fracture surface of side grooved mini-bar EUROFER 97 specimen (EF56).

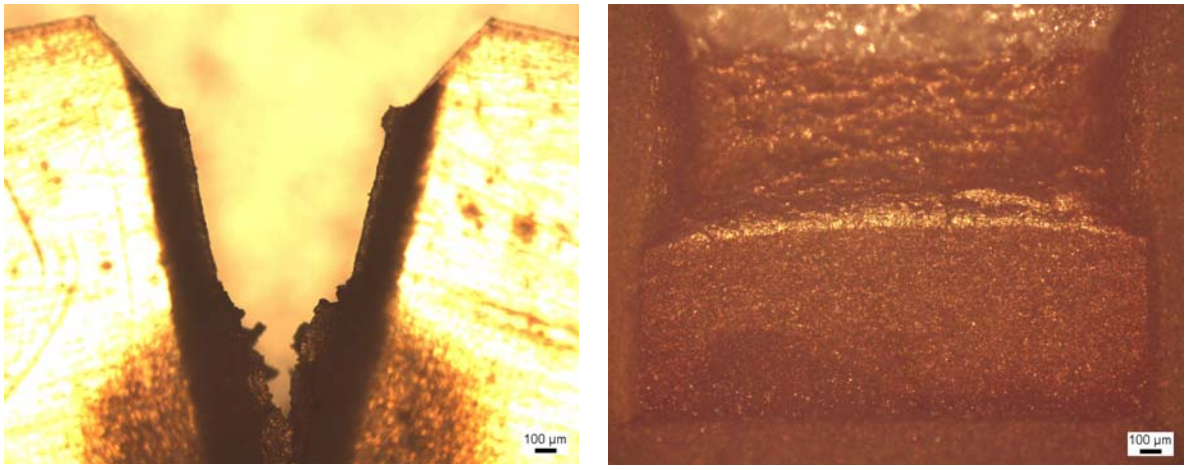

Fig. 6-6 (left) Side view of side grooved mini-bar EUROFER 97 specimen (EF67); Starter notch type “V”; $a_0/W \approx 0.34$; (right) Fracture surface of side grooved mini-bar EUROFER 97 specimen (EF67).

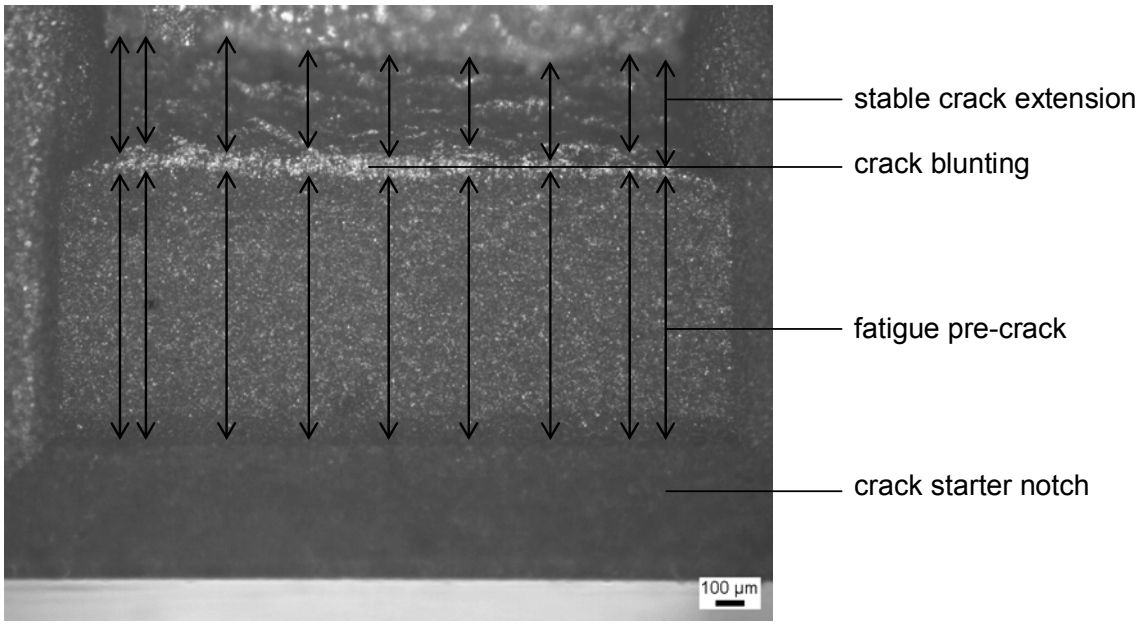

Fig. 6-7 Fracture surface of side grooved mini-bar EUROFER 97 specimen (EF69). Starter notch type "V"; $a_0/W \approx 0.35$; Vertical arrows (separated by crack blunting area in vertical direction) indicate the paths used for assessments of fatigue pre-crack lengths and stable crack extensions.

Specimen	Length (mm)	Net Thickness (mm)	Height (mm)	Starter notch	a_0 (mm)	Δa^* (mm)	U (Nmm)	J (N/mm)
EF63	27	2.37	4	"V"	1.440	0.046	448	148
EF64	27	2.38	4	"V"	1.424	0.071	668	218
EF69	27	2.34	4	"V"	1.403	0.340	1221	402
EF66	27	2.36	4	"V"	1.350	0.471	1540	492
EF65	27	2.37	4	"V"	1.428	0.545	1640	538
EF67	27	2.35	4	"V"	1.345	0.746	1906	612
EF68	27	2.38	4	"V"	1.450	0.850	2026	668

Table 6-3 Quasi-static *three-point-bend* testing of side grooved mini-bar EUROFER 97 specimens; a_0 original crack length; Δa^* in-plane component of stable crack extension; *U* deformation energy.

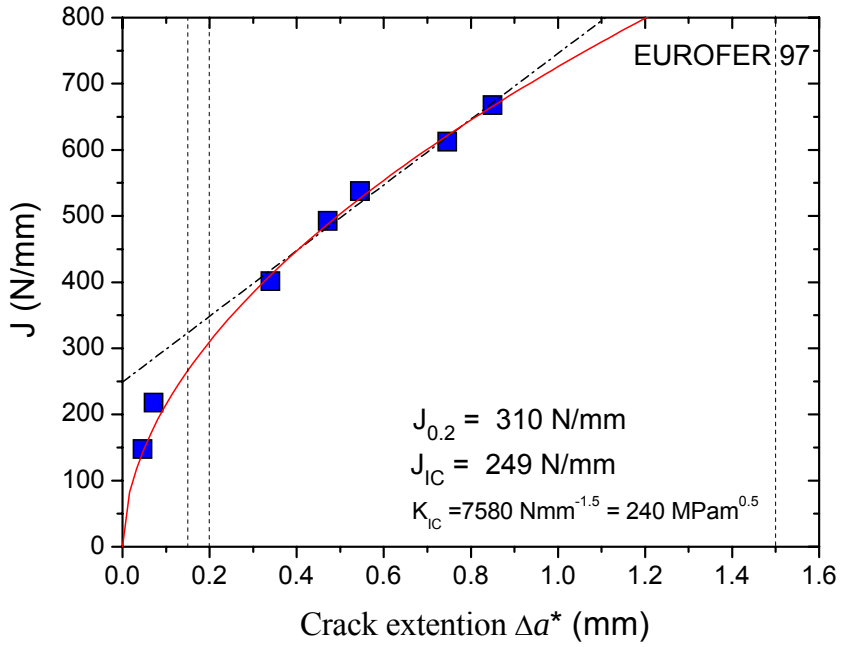

Fig. 6-8 J-Δa curve for EUROFER 97. The solid line is a least square fit according to Eq. (3) for data points fulfilling $0.15 \le \Delta a \le 1.5$ mm criteria; The best fit was obtained with C=726 and p=0.53. Estimated $J_{0.2}$ = 310 N/mm; The dashed dotted line is a linear fit to data points fulfilling $0.15 \le \Delta a \le 1.5$ mm criteria. Estimated J_{IC} = 249 N/mm.

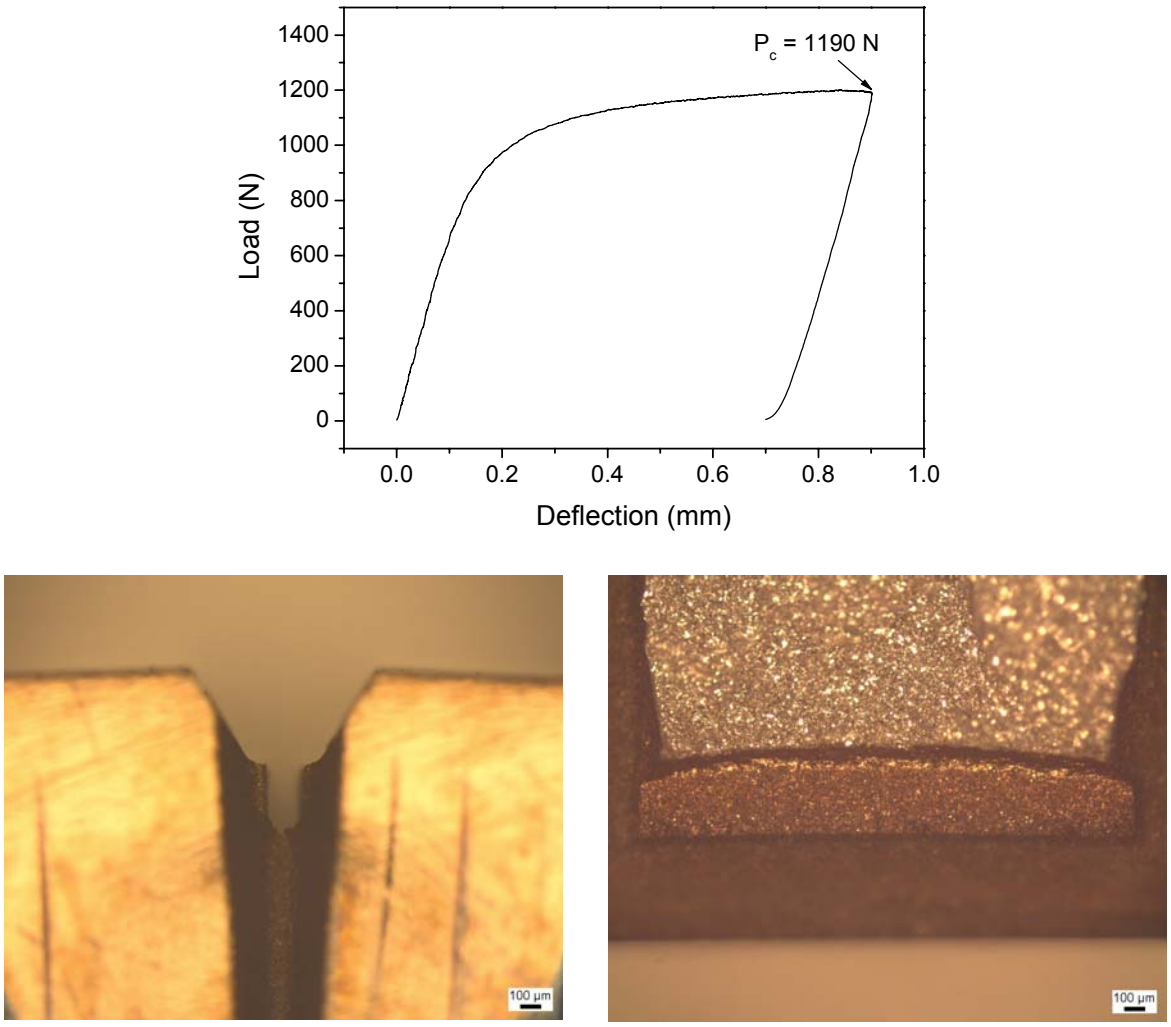

Fig. 6-9 (top) Load vs. deflection curve for EUROFER 97 mini-bar specimen (EF55) loaded to a load-level (P_c) leading to a macroscopic appearance of crack initiation; (bottom, left) Side view of EF55; (bottom, right) Fracture surface of EF55.

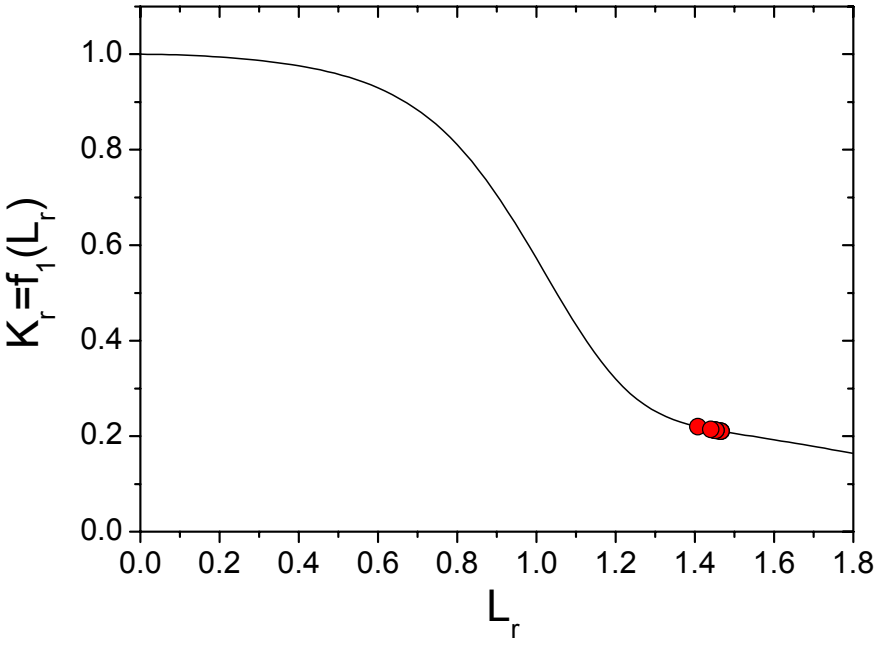

Fig. 6-10 Option 1 curve (solid line) for EUROFER 97 calculated with Eq. (8); The circles indicate L_r values for the specimens deformed to load-levels (P_c) leading to a macroscopic appearance of crack initiation; σ_y(RT) = 537 N/mm^2.

specimen	a_0/W	f(a_0/W)	Starter Notch	B (mm)	B_N (mm)	P_c (N)	P_L (N)	L_r (P_c)	K_{IC} (MPam$^{0.5}$)
EF33	0.237	1.405	"U"	3	3	1207	833.1	1.45	252
EF34	0.232	1.383	"U"	3	3	1236	845.7	1.46	256
EF36	0.237	1.405	"U"	3	3	1201	834.0	1.44	249
EF53	0.230	1.377	"V"	3	2.36	1060	753.0	1.41	237
EF55	0.201	1.271	"V"	3	2.36	1190	811.5	1.47	256
EF57	0.244	1.430	"V"	3	2.36	1064	725.9	1.47	258
EF58	0.237	1.404	"V"	3	2.36	1075	739.4	1.45	254
EF63	0.360	1.914	"V"	3	2.37	755	521.3	1.45	241
EF64	0.356	1.894	"V"	3	2.38	769	529.0	1.45	244

Table 6-4 Selected EUROFER 97 mini-bar specimens (3x4x27 mm^3) deformed to load-levels (P_c) leading to a macroscopic appearance of crack initiation; K_{IC} values are calculated from Eq. (5) assuming the validity of option 1 curve Eq. (8); σ_y(RT) = 537 N/mm^2.

6.5 Experimental results – MANET II

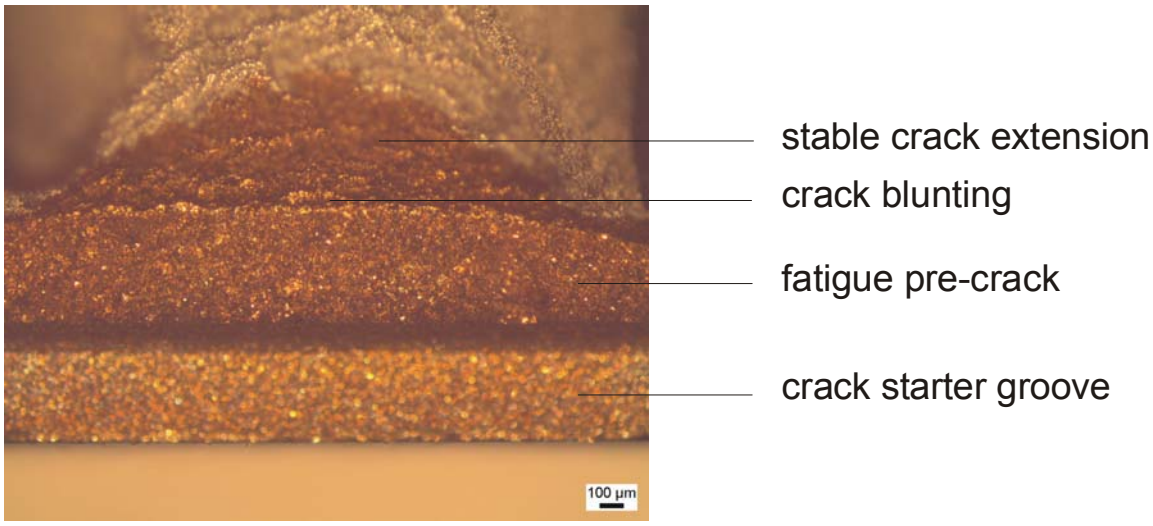

Fig. 6-11 Fracture surface of mini-bar MANET II specimen (H709); ″U″-type starter notch.

Specimen	Length (mm)	Thickness (mm)	Height (mm)	Starter notch	a_0 (mm)	Δa (mm)	U (N·mm)	J (N/mm)
H701	27	3	4	“U”	0.94	0	113.1	24.7
H702	27	3	4	“U”	0.87	0	138.1	29.4
H704	27	3	4	“U”	0.93	0	165.4	35.9
H707	27	3	4	“U”	0.88	0.08	827.5	177.0
H708	27	3	4	“U”	0.91	0.17	1400.6	302.5
H709	27	3	4	“U”	0.91	0.21	1555.0	335.5
H712	27	3	4	“U”	0.84	0.27	1959.0	413.3
H710	27	3	4	“U”	0.95	0.45	2209.0	482.2
H711	27	3	4	“U”	0.86	0.76	2817.0	597.9

Table 6-5 Quasi-static *three-point-bend* testing of MANET II mini-bar specimens; a_0 original crack length; Δa stable crack extension; U deformation energy.

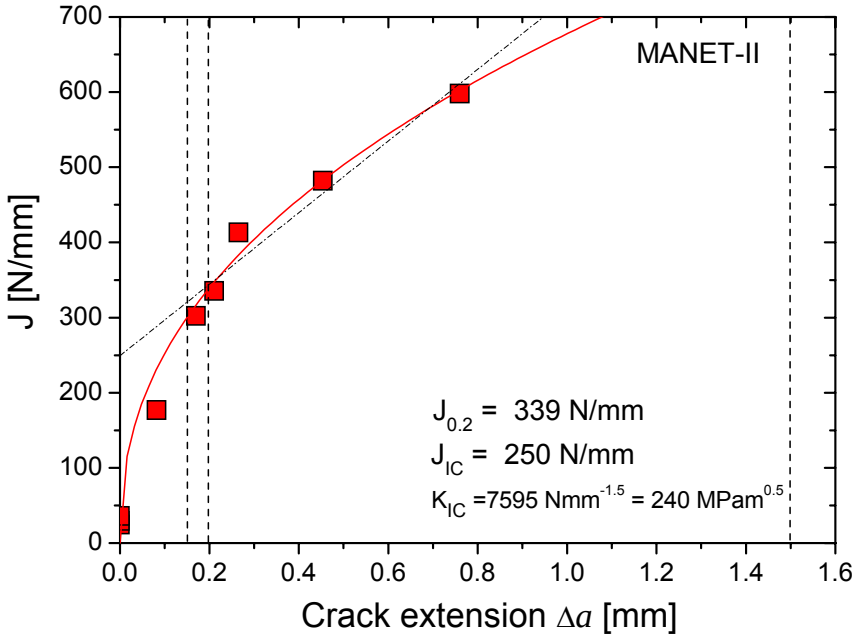

Fig. 6-12 J-Δa curve for MANET II; The solid line is a least square fit according to Eq. (3) for data points fulfilling $0.15 \le \Delta a \le 1.5$ mm criteria; The best fit was obtained with parameters C=678 and p=0.43; Estimated $J_{0.2}$ = 339 N/mm; The dashed-dotted line is a linear fit to data points fulfilling $0.15 \le \Delta a \le 1.5$ mm criteria; Estimated J_{IC} = 250 N/mm.